D-A-D-type Bilophine Derivative-Based Photoactive Metal-Organic Framework: Fluorescence Sensing of UO_2^{2+} and Photochromic Behavior

Yu-jian Cheng[a], Zi-tong Chen[a,*], Hao-ran Ji[a], Yuan Chen[a,*], Bao Li[a, b*]

[a] Key Laboratory of Material Chemistry for Energy Conversion and Storage, Semiconductor chemistry center, School of Chemistry and Chemical Engineering, Hubei Key Laboratory of Bioinorganic Chemistry & Materia Medica, Huazhong University of Science and Technology, Wuhan, Hubei, 430074, People's Republic of China. Email: chenzncu0514@163.com, chenyuan122800@163.com, libao@hust.edu.cn.

[b]Jiangxi Provincial Key Laboratory of Functional Crystalline Materials Chemistry, Jiangxi University of Science and Technology, Ganzhou 341000, Jiangxi Province, P.R. China.

Luminescence detection of different anions.

Then, the potential of Cd-MOF as a luminescence sensor for the detection of inorganic anions, including Cl^-, Br^-, I^-, NO_2^-, SCN^-, SO_4^{2-}, IO_3^-, CrO_4^{2-}, $Cr_2O_7^{2-}$ and MnO_4^- was explored. As shown in Fig. S4, the composite system containing CrO_4^{2-}, $Cr_2O_7^{2-}$ and MnO_4^- exhibited a strong fluorescence quenching effect with quenching efficiencies of 96, 100, and 100%, respectively. The results of competition experiments showed that the fluorescence quenching efficiency of Cd-MOF was almost unaffected in CrO_4^{2-}, $Cr_2O_7^{2-}$ and MnO_4^- solutions containing other anions (Fig. S8). According to the S-V curves, as shown in Fig. S17, CrO_4^{2-} and MnO_4^- showed good linearity over the whole concentration range of 0-14 μM and 0-8 μM and lower detection concentration intervals, respectively. K_{sv} values of 2.4×10^4 and 7.1×10^4 M^{-1}, the S-V curves of $Cr_2O_7^{2-}$ showed good linearity in the concentration range of 0-60 μM, and the fluorescence quenching constant, K_{sv}, was 1.7×10^4 M^{-1}, which indicated that the effect of Cd-MOF on CrO_4^{2-}, $Cr_2O_7^{2-}$ and MnO_4^- with good detection performance.

Luminescent detection of antibiotics.

The widespread use of antibiotics has contributed to the development of sensors for the detection of antibiotic residues in the environment. The effectiveness of Cd-MOF in antibiotic detection was also tried. Nine antibiotics, including sulfadiazine (SDZ), sulfamethoxazole (SMZ), sulfamethoxazole (SMT), sulfamethoxazole (TAP), enrofloxacin (ENR), norfloxacin (NOR), furazolidone (FZD), furazanidazole (NFZ), and tetracycline (TC), were selected as analytes.[1, 2] The Cd-MOF was tested for the detection of antibiotic residues in the environment at the same excitation wavelength at room temperature ($\lambda_{ex} = 360$ nm), the fluorescence spectra of Cd-MOF in different antibiotic solutions were tested.

SDZ, SMZ, SMT, and TAP had fluorescence intensity enhancement effects on Cd-MOF, and the remaining antibiotics ENR, NOR, FZD, NFZ, and TC had different degrees of quenching effects on the fluorescence intensity of Cd-MFO (Fig. S5). The order of the quenching efficiency from high to low was TC > NFZ > FZD > NOR > ENR, all of which could achieve a quenching efficiency of more than 80%.

Luminescent detection of nitro explosives.

Nitroaromatic compounds are important synthetic raw materials in industry, as well as in pharmaceuticals and dyes.[3, 4] Exposure of nitroaromatic compounds, such as nitrobenzene (NB) and 2,4,6-trinitrophenol (TNP), to the environment can result in serious environmental pollution. Therefore, the feasibility of Cd-MOF for the detection of nitro explosives including nitrobenzene (NB), 1,3-dinitrobenzene (1,3-DNB), 1,4-dinitrobenzene (1,4-DNB), 2,4-dinitrotoluene (2,4-DNT), 4-nitrophenol (4-NP), 2-nitrotoluene (2-NT), and 2,4,6-trinitrophenol (TNP). The fluorescence intensity reduction of Cd-MOF by generic nitroaromatic explosives was different (Fig. S6). The most significant quenching effect was 4-NP, followed by TNP, while the rest of the nitroaromatic explosives showed relatively weak quenching effects.

Table S1. Crystal data and structure refinement for Cd-MOF.

Identification code	Cd-MOF
Empirical formula	$C_{40}H_{22}N_4O_8Cd$
Formula weight	799.03
Temperature/K	273.15
Crystal system	monoclinic
Space group	$C2/c$
a/Å	20.0697(7)
b/Å	18.6744(6)
c/Å	13.6622(4)
α/°	90
β/°	103.4630(10)
γ/°	90
Volume/Å^3	4979.7(3)
Z	4
ρ_{calc}g/cm^3	1.063
μ/mm^{-1}	0.481
F(000)	1600.0
Radiation	MoKα ($\lambda = 0.71073$)
2θ range for data collection/°	3.018 to 46.542
Index ranges	$-22 \leq h \leq 22, -20 \leq k \leq 20, -15 \leq l \leq 15$
Reflections collected	19707
Independent reflections	3463 [$R_{int} = 0.0612$, $R_{sigma} = 0.0414$]
Data/restraints/parameters	3463/0/240
Goodness-of-fit on F^2	1.126
Final R indexes [I $\geq$ 2σ (I)]	$R_1 = 0.0616$, $wR_2 = 0.1868$
Final R indexes [all data]	$R_1 = 0.0644$, $wR_2 = 0.1971$

Table S2. Bond Lengths for Cd-MOF.

Atom	Atom	Length/Å	Atom	Atom	Length/Å
Cd1	O4[1]	2.454(4)	C13	C14	1.457(8)
Cd1	O4[2]	2.454(4)	C12	C11	1.479(8)
Cd1	O1	2.244(4)	C15	C16	1.387(8)
Cd1	O1[3]	2.244(4)	C15	C14	1.393(8)
Cd1	O3[2]	2.321(5)	O2	C20	1.217(9)
Cd1	O3[1]	2.321(5)	C19	C16	1.382(9)
Cd1	C1[2]	2.733(6)	C19	C20	1.505(9)
Cd1	C1[1]	2.733(6)	C19	C18	1.388(10)
O4	C1	1.252(7)	C11	C9	1.373(9)
O1	C20	1.242(9)	C11	C10	1.361(9)
N1	C8	1.386(8)	C6	C5	1.401(9)
N1	C12	1.366(8)	C5	C2	1.376(10)
N2	C13	1.395(8)	C4	C3	1.387(9)
N2	C12	1.309(8)	C2	C1	1.502(9)
O3	C1	1.229(8)	C2	C3	1.374(10)
C8	C7	1.468(8)	C14	C17	1.395(9)
C8	C13	1.387(9)	C9	C10[4]	1.422(9)
C7	C6	1.372(9)	C18	C17	1.375(9)
C7	C4	1.390(9)			

[1]-1/2+X,-1/2+Y,+Z; [2]3/2-X,-1/2+Y,3/2-Z; [3]1-X,+Y,3/2-Z; [4]3/2-X,1/2-Y,-Z

Table S3. Bond Angles for Cd-MOF.

Atom	Atom	Atom	Angle/°	Atom	Atom	Atom	Angle/°
O4[1]	Cd1	O4[2]	123.9(2)	O3[1]	Cd1	O4[1]	53.82(15)
O4[2]	Cd1	C1[2]	27.26(16)	O3[1]	Cd1	O3[2]	89.1(4)
O4[2]	Cd1	C1[1]	105.83(18)	O3[1]	Cd1	C1[2]	87.8(2)
O4[1]	Cd1	C1[2]	105.83(18)	O3[2]	Cd1	C1[2]	26.58(18)
O4[1]	Cd1	C1[1]	27.26(16)	O3[1]	Cd1	C1[1]	26.58(18)
O1	Cd1	O4[2]	81.15(15)	O3[2]	Cd1	C1[1]	87.8(2)
O1[3]	Cd1	O4[2]	138.04(16)	C1[1]	Cd1	C1[2]	98.2(3)
O1	Cd1	O4[1]	138.04(16)	C1	O4	Cd1[4]	88.8(4)
O1[3]	Cd1	O4[1]	81.15(15)	C20	O1	Cd1	105.9(4)
O1	Cd1	O1[3]	102.3(2)	C1	O3	Cd1[4]	95.8(4)
O1[3]	Cd1	O3[2]	102.50(18)	N1	C8	C7	120.2(5)
O1	Cd1	O3[2]	132.61(19)	N1	C8	C13	105.5(5)
O1[3]	Cd1	O3[1]	132.61(19)	O4	C1	Cd1[4]	63.9(3)
O1	Cd1	O3[1]	102.50(18)	O4	C1	C2	119.2(6)
O1[3]	Cd1	C1[2]	121.76(18)	O3	C1	Cd1[4]	57.7(3)
O1[3]	Cd1	C1[1]	107.16(18)	O3	C1	O4	121.5(6)
O1	Cd1	C1[2]	107.16(18)	O3	C1	C2	119.3(6)
O1	Cd1	C1[1]	121.76(18)	C2	C1	Cd1[4]	175.1(5)
O3[2]	Cd1	O4[2]	53.82(15)	O1	C20	C19	118.5(6)
O3[1]	Cd1	O4[2]	85.4(2)	O2	C20	O1	121.8(7)
O3[2]	Cd1	O4[1]	85.4(2)	O2	C20	C19	119.7(7)

[1]-1/2+X,-1/2+Y,+Z; [2]3/2-X,-1/2+Y,3/2-Z; [3]1-X,+Y,3/2-Z; [4]1/2+X,1/2+Y,+Z; [5]3/2-X,1/2-Y,-Z
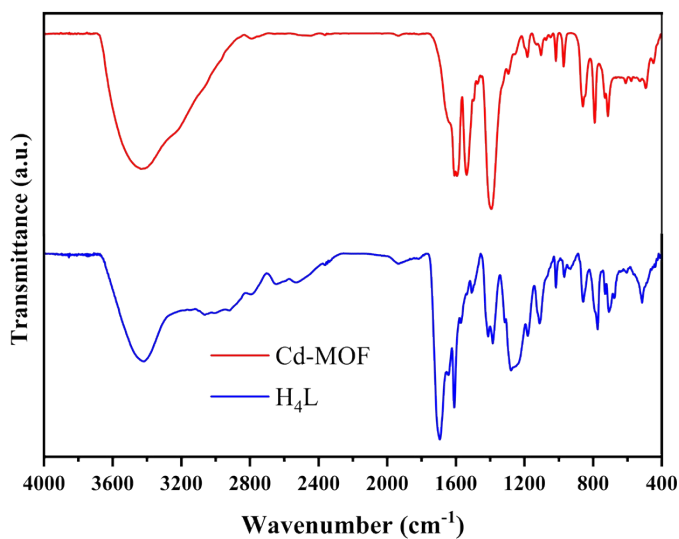
Figure S1. Infrared spectra of H_4L and Cd-MOF.
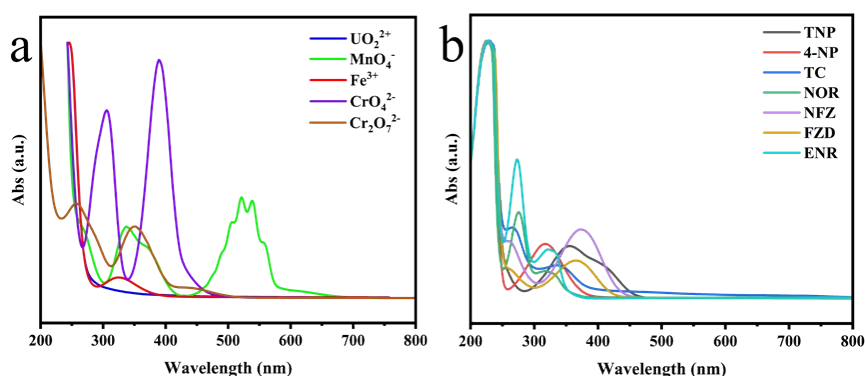
Figure S2. UV-visible absorption spectra of anions and cations undergoing fluorescence quenching (a), nitro explosives, and antibiotics (b).
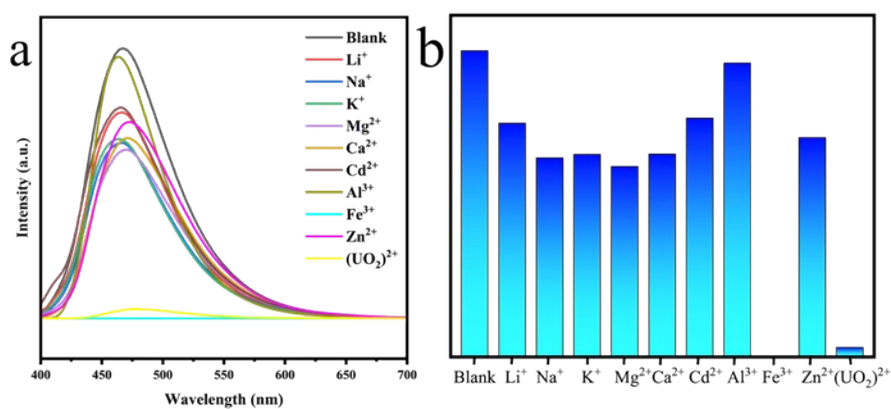
Figure S3. Cation quenching curves of Cd-MOF (a), and histogram of cation quenching percentage of cations (b).
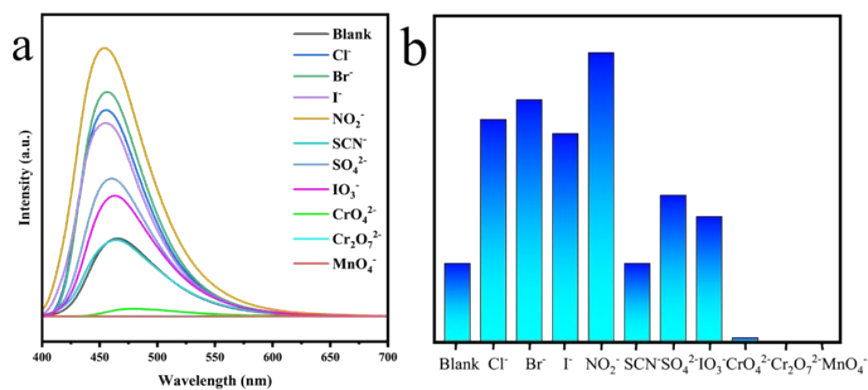
Figure S4. Anion quenching curve of Cd-MOF (a), and histogram of quenching percentage of anions (b).
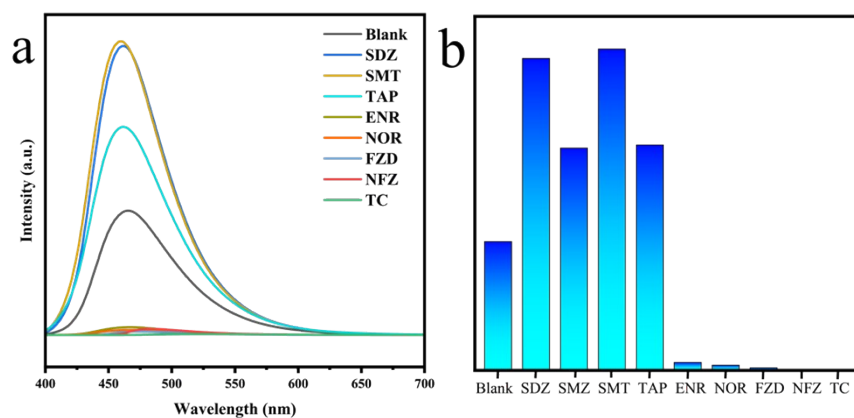

Figure S5. Antibiotic quenching curve of Cd-MOF (a), and histogram of percentage quenching of antibiotics (b).
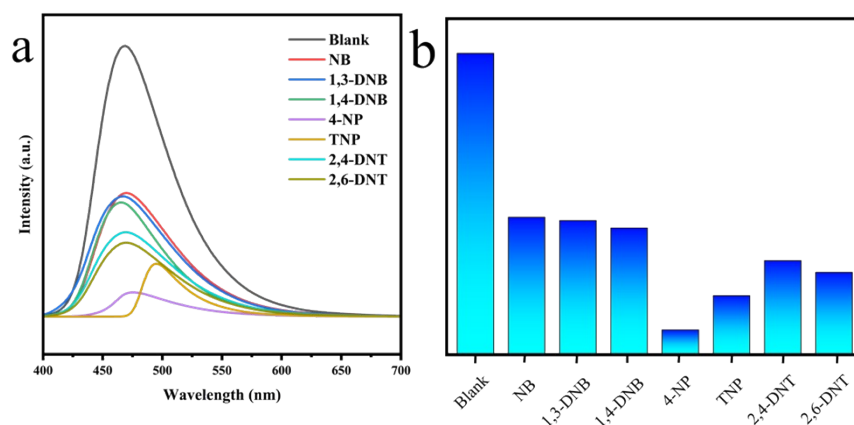
Figure S6. Nitro explosive quenching curve for Cd-MOF (a), and histogram of the percentage quenching of nitro explosives (b).
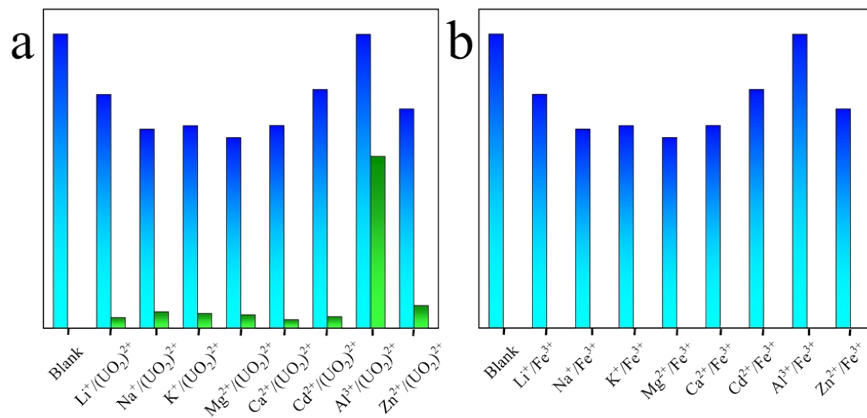
Figure S7. Histograms of fluorescence intensity of Cd-MOF for the detection of UO_2^{2+} (a) and Fe^{3+} (b) under different metal ion interferences.
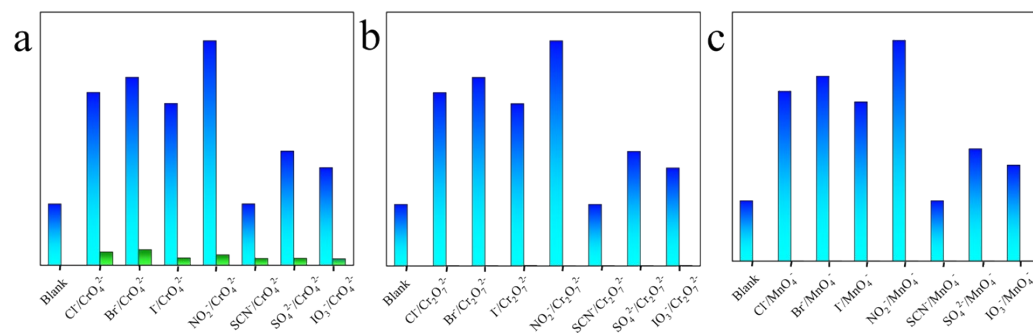
Figure S8. Histograms of fluorescence intensity of CrO_4^{2-} (a), $Cr_2O_7^{2-}$ (b) and MnO_4^- (c) detected by Cd-MOF under different anionic interferences.
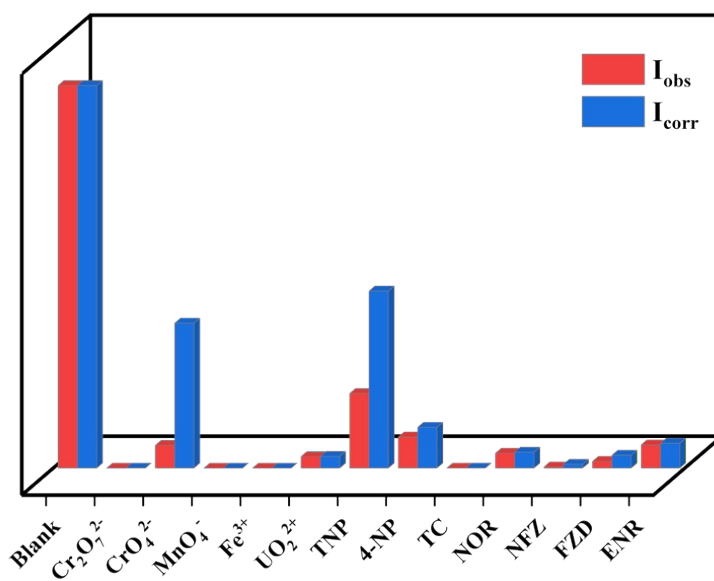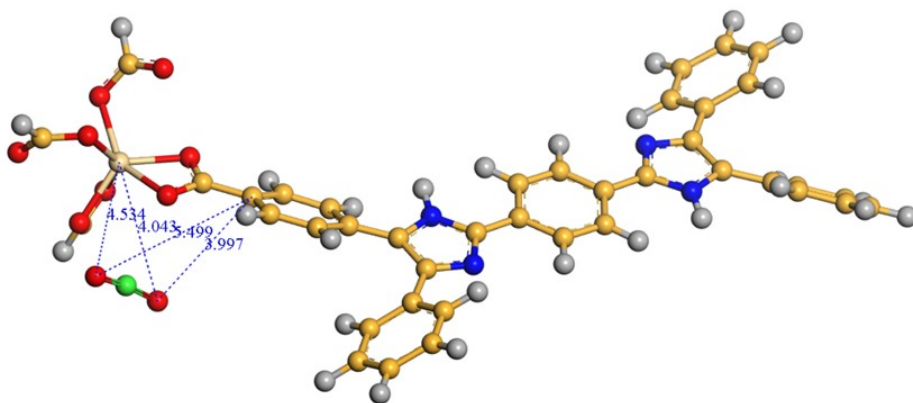
Figure S10. Distance between UO_2^{2+} and Cd-MOF.
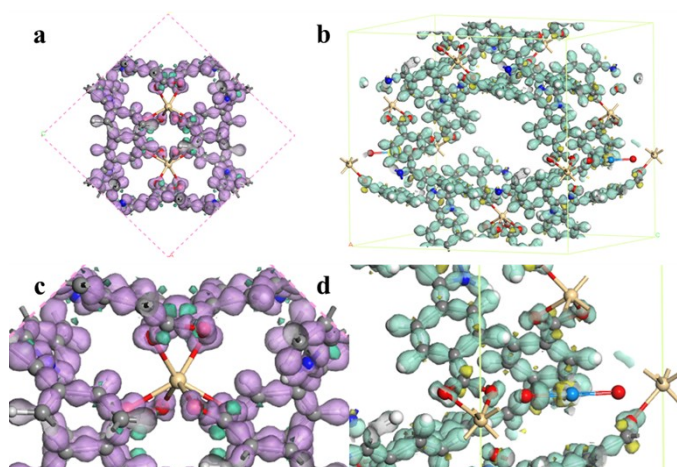
Figure S11. Differential electron density plots and zoomed-in plots for Cd-MOF (a, c) and UO_2^{2+}@Cd-MOF (b, d), respectively.
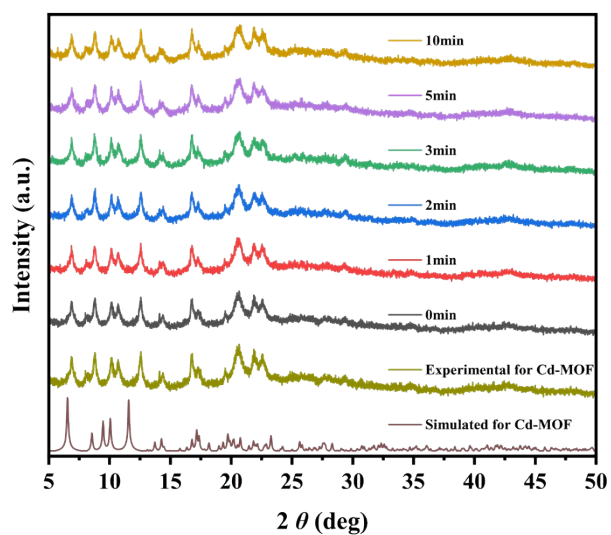
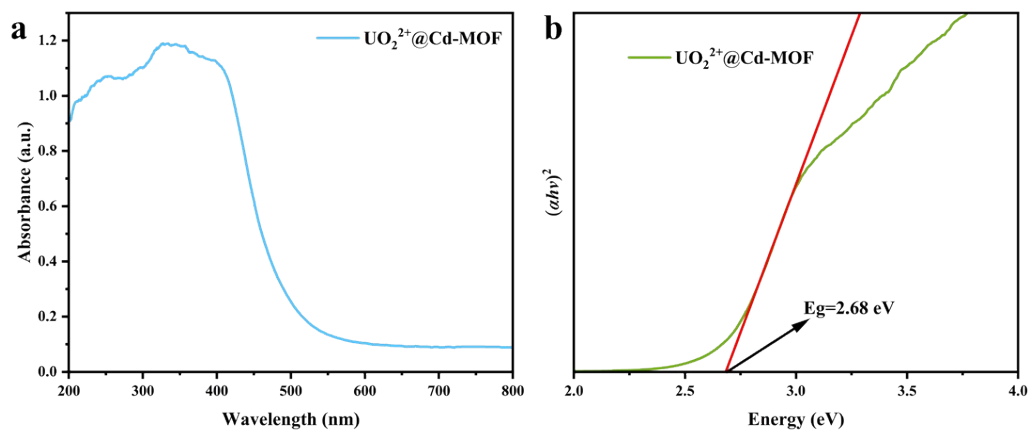**Figure S12.** The XRD diffraction of Cd-MOF under irradiation.
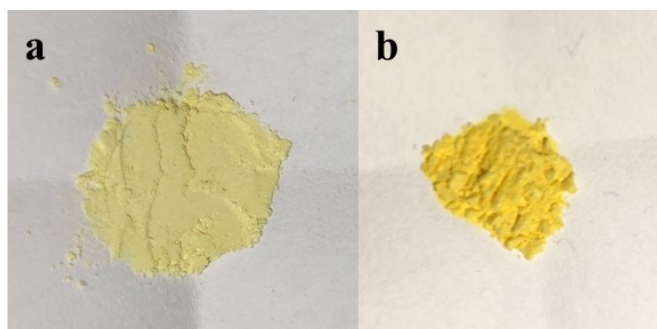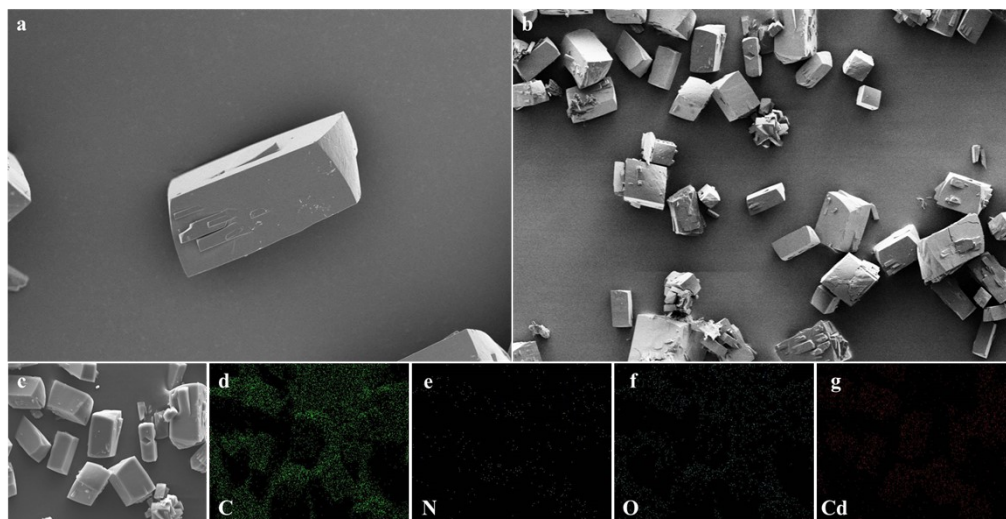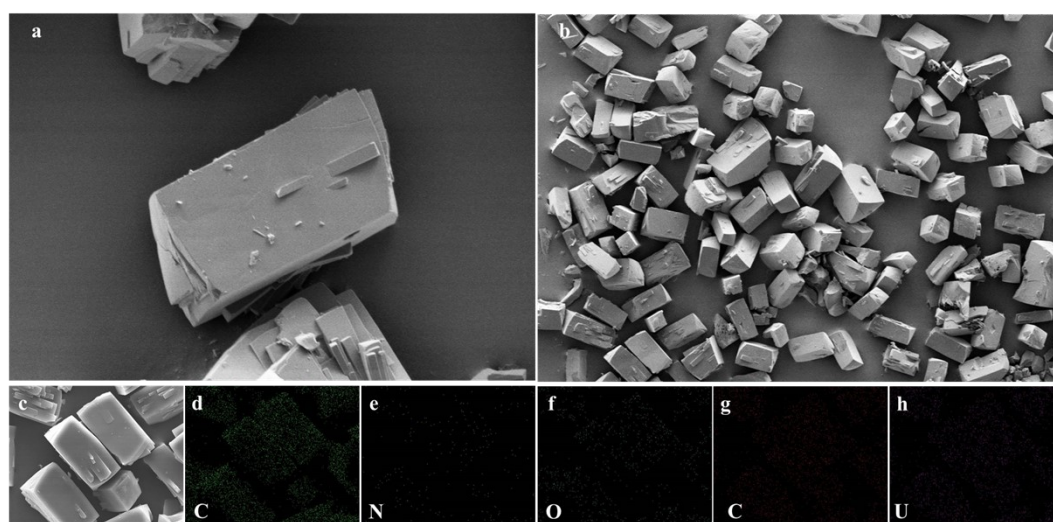
Figure S16. (a) UV-visible diffuse reflectance spectra and (b) the corrsponding Tauc plot of $UO_2^{2+}@Cd-MOF$.
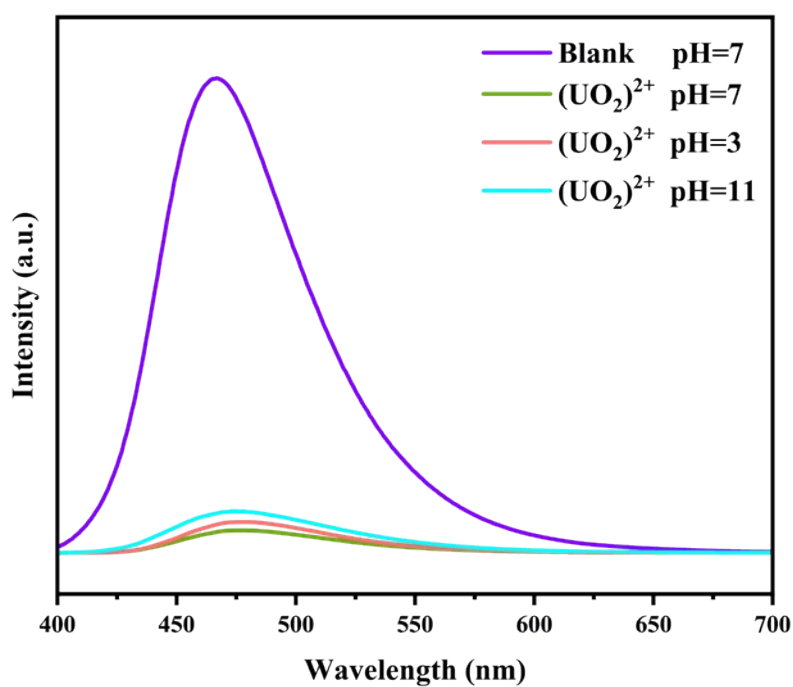

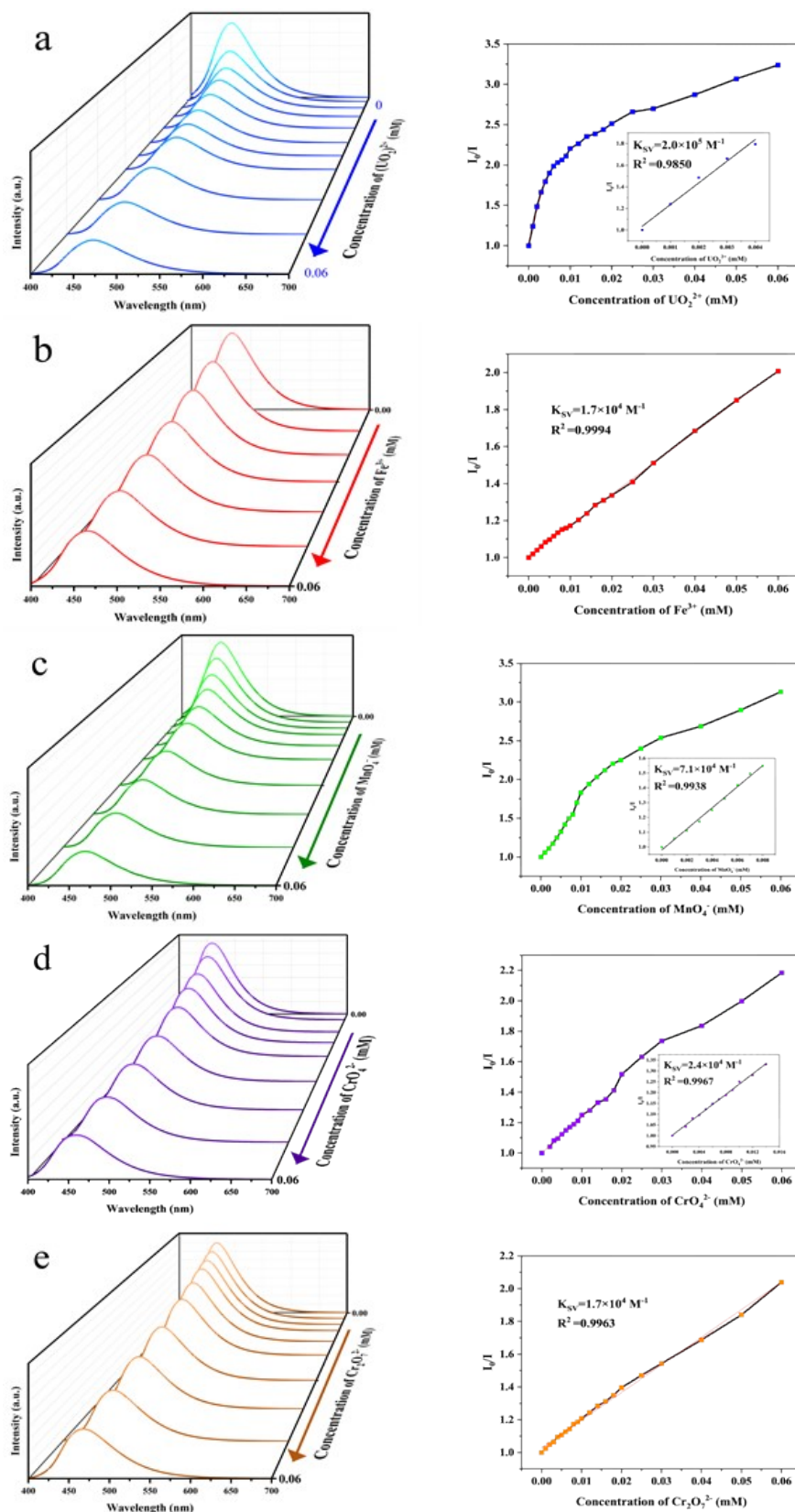**Figure S16.** Fluorescence quenching curves of Cd-MOF in simulated seawater at different pH conditions.

Figure S17. Fluorescence spectra of Cd-MOF in solutions of (a) UO_2^{2+}, (b) Fe^{3+}, (c) MnO_4^-, (d) CrO_4^{2-} and (e) $Cr_2O_7^{2-}$ at different concentrations and the corresponding linearity.

References

1. L. Lan Men, J. Li, M. Yue Fan, X. Li, Y. Ling Liu, F. Wei Gao and Z. Min Su, Anthracene-Modified Cadmium Metal-Organic Framework as an Excellent Sensor for the Detection of 2,4,6-Trinitrophenol and Nitrofurantoin, *Eur. J. Inorg. Chem.*, 2022, **2022**, e202100999.

2. Y.-L. Zhao, Q. Chen, J. Lv, M.-M. Xu, X. Zhang and J.-R. Li, Specific sensing of antibiotics with metal-organic frameworks based dual sensor system, *Nano Res.*, 2022, **15**, 6430-6437.

3. J.-L. Li, Y. Xiao, L.-Y. Wang, Y.-H. Xing, F.-Y. Bai and Z. Shi, Oriented construction of the Mixed-metal organic framework with triazine hexacarboxylic acid and fluorescence detection: Fe^{3+}, $Cr_2O_7^{2-}$ and TNP, *Polyhedron*, 2022, **214**, 115648.

4. S. A. A. Razavi, A. Morsali and M. Piroozzadeh, A Dihydrotetrazine-Functionalized Metal–Organic Framework as a Highly Selective Luminescent Host–Guest Sensor for Detection of 2,4,6-Trinitrophenol, *Inorg. Chem.*, 2022, **61**, 7820-7834.